Applied Numerical Mathematics 143 (2019) 20–34

Contents lists available at ScienceDirect

Applied Numerical Mathematics

www.elsevier.com/locate/apnum

A nonlinear least squares framework for periodic grating identification with a high–order perturbation of surfaces implementation

Matthew Kaplan, David P. Nicholls *

Department of Mathematics, Statistics, and Computer Science, University of Illinois at Chicago, Chicago, IL 60607, United States of America

ARTICLE INFO

Article history:
Received 16 July 2018
Received in revised form 15 January 2019
Accepted 7 March 2019
Available online 29 March 2019

Keywords:
Inverse problems
Grating identification
High–order perturbation of surfaces methods
Gauss–Newton algorithm
Levenberg–Marquardt algorithm
Frequency–domain electromagnetics

ABSTRACT

The scattering of linear electromagnetic waves by a layered structure is a central model in many problems of engineering interest. In this contribution, we focus on the interaction of visible and near–visible radiation with periodic structures on the micron or nanometer scales which are relevant for many applications in nanoplasmonics. The fabrication of such structures is extremely difficult and costly, and even the most sophisticated laboratories have difficulty measuring the dimensions of gratings they have constructed. We present a new, extremely rapid and robust, identification algorithm for providing precisely this information. It is built upon a Nonlinear Least Squares framework, and implemented with a High–Order Perturbation of Surfaces methodology which is orders of magnitude faster than volumetric solvers, while outperforming surface methods (such as Boundary Integral Methods) for the geometries we consider here. In addition to a full derivation and specification of the algorithm, we also support our claims with a number of illustrative simulations.

1. Introduction

The scattering of linear electromagnetic waves by a layered structure is a central model in many problems of engineering interest. From surface enhanced Raman scattering [96] and extraordinary optical transmission [34], to surface enhanced spectroscopy [73] and plasmon resonance biosensing [49,65], examples abound. In this contribution, we focus on the interaction of visible and near–visible radiation with periodic structures on the micron or nanometer scales which is relevant for many applications in nanoplasmonics [91,66,38].

The fabrication of such structures is extremely difficult and costly [55,59,65,74], and even the most sophisticated laboratories have difficulty measuring the dimensions of gratings they have constructed. We present a new, extremely rapid and robust, identification algorithm for providing precisely this information. It is built upon a Nonlinear Least Squares (NLSQ) framework and implemented with a High–Order Perturbation of Surfaces (HOPS) methodology which is orders of magnitude faster than volumetric solvers, while outperforming surface methods (such as Boundary Integral Methods) for the geometries we consider here.

A commonly used structure in applications consists of a doubly layered diffraction grating composed of a metal (e.g., gold or silver) overlaid with a dielectric (e.g., air or water) featuring a periodically corrugated interface [91,66,38]. With this

* Corresponding author.
E-mail addresses: mkapla21@uic.edu (M. Kaplan), davidn@uic.edu (D.P. Nicholls).

https://doi.org/10.1016/j.apnum.2019.03.012
0168-9274/

model in mind, we take as given that the constituent materials are known together with the period, and can now ponder two important and related questions:

1. Given the shape of the interface, can one compute scattering quantities given incident radiation?
2. Having specified incident waves and measured scattering returns, can one deduce information about the interface shape between the two layers?

In this paper we take up the latter question and propose a novel algorithm for this. Our method is based upon a HOPS algorithm, the method of Field Expansions (FE) [18–20], which is not only rapid and robust, but also ideally suited to the scaling regime under consideration here.

In the engineering literature there is a preponderance of volumetric approaches to these problems with a particular focus upon Finite Difference [64], Finite Element [57], Discontinuous Galerkin [46], Spectral Element [33], and Spectral [43,95] methods. Clearly, such methods are disadvantaged with an unnecessarily large number of degrees of freedom for the piecewise homogeneous problem we consider here. Additionally, the correct application of outgoing wave conditions is an issue. This complication typically necessitates approximation, e.g., with a Perfectly Matched Layer [9,10] or an exact, non–reflecting boundary condition [58,45,60,42,78,11] which spoils the sparseness properties of the relevant linear systems.

Due to these factors, surface methods are an appealing choice as they are orders of magnitude quicker than volumetric approaches because of the greatly reduced number of unknowns required to resolve a computation. In addition, far–field boundary conditions are enforced exactly through the choice of the Green function. As such, these methods are a compelling alternative which are gaining favor with engineers. The most prevalent among these interfacial algorithms are Boundary Integral Methods [32,93], but these face difficulties as well. Most have been resolved in recent years through (i.) the use of sophisticated quadrature rules to deliver High–Order Spectral (HOS) accuracy; (ii.) the design of preconditioned iterative solvers with suitable acceleration [44]; (iii) new strategies to accelerate the convergence of the periodized Green function [17,16] (or avoiding its periodization entirely [8,30]); and (iv.) new approaches to deal with the Rayleigh singularities (widely known in the literature as "Wood's anomalies") [14,15,25]. Consequently, they are a tempting alternative for many problems of applied interest, however, they can be disadvantaged for the class of problems we consider as compared with the methods we advocate here due to the dense, non–symmetric positive definite systems of linear equations that must be solved with each simulation.

In contrast, a HOPS methodology effectively addresses this concern. These algorithms have the advantageous properties of BIM formulations (e.g., surface formulation, reduced numbers of unknowns, and exactly outgoing solutions) while being immune to the criticism listed above: The scheme is built upon the flat–interface solution which is trivially solved in Fourier space by inverting a *sparse* operator at each wavenumber. We point out that the implied smallness assumption on the deformation can be dropped in light of the analytic continuation results in [81,54] which demonstrate that the domain of analyticity contains a neighborhood of the *entire* real axis. Therefore, with appropriate numerical analytic continuation strategies (e.g., Padé approximation [2]) to access this region of analyticity, quite large and irregular perturbations can be simulated. We direct the interested reader to [19,21,24,79,82] for numerical demonstrations.

There are many HOPS algorithms for the solution of partial differential equations posed on irregular domains, but they all originate in classical low–order calculations such as those of Rayleigh [92] and Rice [94]. The first high–order approaches were the Operator Expansions (OE) method of Milder [69–72] and FE method of Bruno and Reitich [18–20]. Each has been enhanced by various authors, but the most significant was the stabilization of these methods by one of the authors and Reitich with the Transformed Field Expansions (TFE) algorithm [80,79,81,83,82]. Beyond this, these HOPS schemes have been extended in a number of directions. For instance for bounded obstacle configurations [23,84,39], the full vector Maxwell equations [22,75,88], and multiply layered media [50–52]. For a rigorous numerical analysis please see [85].

Focusing on the inverse problem, a vast amount of work has been conducted on this problem and one can consult any one of the following reference texts for more details [28,32,63,26,27]. The paper of Jiang and Li [56] gives a nice survey of previous results on this topic with specific application to the two–dimensional periodic grating structures under consideration here. Their paper includes the following citations (included for the reader's convenience) on uniqueness and stability [3,4,62,48,12], and assorted computational approaches [36,37,47,13,35,1,7]. Of special note is the extensive line of work of Li and collaborators on inversion strategies based upon HOPS methods (in particular the TFE algorithm [82]). More specifically, they describe techniques for phaseless data [5,99] and near–field measurement [29,6].

Our inversion strategy is inspired by the work of one of the authors and Taber [86,87] on the recovery of topography shape under a layer of an ideal fluid (e.g., the ocean), and the discovery of sediment layer shapes from acoustic signals in a geoscience inversion strategy outlined by one of the authors and Malcolm [67,68]. In each of these, rather explicit formulas for HOPS expansions of surface integral operators (Dirichlet–Neumann Operators) were used to identify relations involving the interface shape which could be *iterated* to produce a form which best explained the data observed. While we also use HOPS methods in the current contribution, we do not rely heavily upon the *specific* forms of the terms in the expansions for our strategy. Instead, we adopt a rather general NLSQ framework [61,89] where we define a particular residual to minimize in a least squares sense. To achieve this we appeal to the well known Gauss–Newton (GN) and Levenberg–Marquardt (LM) algorithms for iteratively minimizing this residual [61,89,98]. As we shall demonstrate, our new approach is quite effective and outperforms our other HOPS schemes by an order of magnitude.

The organization of the paper is as follows: In § 2 we recall the governing equations, and in § 3 we discuss a non–overlapping Domain Decomposition Method (DDM) which is posed in terms of surface unknowns. In § 4 we discuss considerations of the forward problem, while we discuss our inversion strategy in § 5. We conclude with our numerical results in § 6.

2. Governing equations

In Fig. 1 we display the geometry of the configuration we consider: A y–invariant doubly layered structure. An insulator (e.g., vacuum) with refractive index $n^{(u)}$ occupies the domain *above* the graph $z = g(x)$,

$$S^{(u)} := \{z > g(x)\},$$

and a second material with index of refraction $n^{(w)}$ fills

$$S^{(w)} := \{z < g(x)\}.$$

The grating is d–periodic so that $g(x+d) = g(x)$. The structure is illuminated from above by monochromatic plane–wave incident radiation of angular frequency ω, aligned with the grooves

$$\begin{pmatrix} \underline{\mathbf{E}}^i(x,z,t) \\ \underline{\mathbf{H}}^i(x,z,t) \end{pmatrix} = \begin{pmatrix} \mathbf{A} \\ \mathbf{B} \end{pmatrix} e^{i\alpha x - i\gamma^{(u)} z - i\omega t}.$$

We consider the reduced electric and magnetic fields

$$\begin{pmatrix} \mathbf{E}(x,z) \\ \mathbf{H}(x,z) \end{pmatrix} = e^{i\omega t} \begin{pmatrix} \underline{\mathbf{E}}(x,z,t) \\ \underline{\mathbf{H}}(x,z,t) \end{pmatrix},$$

which, like the reduced scattered fields, are α–quasiperiodic due to the incident radiation. Finally, the scattered radiation must be "outgoing" (upward propagating in $S^{(u)}$ and downward propagating in $S^{(w)}$).

As shown in Petit [90], in this two–dimensional setting, the time–harmonic Maxwell equations decouple into two scalar Helmholtz problems which govern the transverse electric (TE) and transverse magnetic (TM) polarizations. We denote the invariant (y) directions of the scattered (electric or magnetic) fields by

$$u = u(x,z), \quad w = w(x,z),$$

in $S^{(u)}$ and $S^{(w)}$, respectively, and the incident radiation in the upper layer by u^i. With this we are led to seek outgoing, α–quasiperiodic solutions of

$$\Delta u + \left(k^{(u)}\right)^2 u = 0, \qquad z > g(x), \tag{2.1a}$$

$$\Delta w + \left(k^{(w)}\right)^2 w = 0, \qquad z < g(x), \tag{2.1b}$$

$$u - w = \zeta, \qquad z = g(x), \tag{2.1c}$$

$$\partial_N u - \tau^2 \partial_N w = \psi, \qquad z = g(x), \tag{2.1d}$$

where $k^{(m)} = n^{(m)}\omega/c$, $(m \in \{u, w\})$, $N = (-\partial_x g, 1)^T$, the Dirichlet and Neumann data are

$$\zeta(x) := -u^i(x, g(x)) = -e^{i\alpha x - i\gamma^{(u)} g(x)},$$

$$\psi(x) := -(\partial_N u^i)(x, g(x)) = \left(i\gamma^{(u)} + i\alpha(\partial_x g)\right) e^{i\alpha x - i\gamma^{(u)} g(x)},$$

and

$$\tau^2 = \begin{cases} 1, & \text{TE}, \\ \left(k^{(u)}/k^{(w)}\right)^2 = \left(n^{(u)}/n^{(w)}\right)^2, & \text{TM}. \end{cases}$$

2.1. Transparent boundary conditions

The Rayleigh expansions [90,97] state that, for $z > |g|_{L^\infty}$, outgoing (upward propagating in $S^{(u)}$) solutions can be expressed as

$$u(x,z) = \sum_{p=-\infty}^{\infty} \hat{u}_p e^{i\alpha_p x} e^{i\gamma_p^{(u)} z}, \tag{2.2}$$

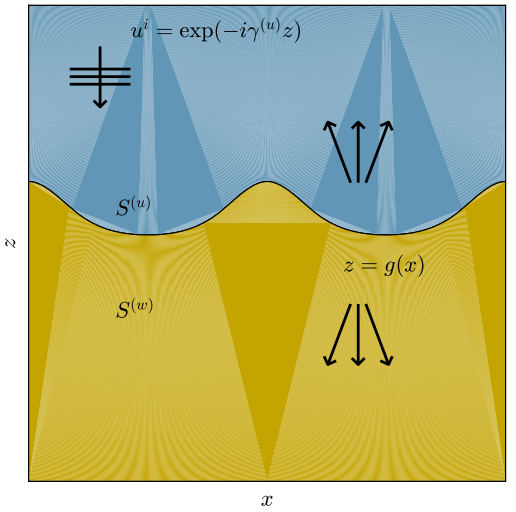

Fig. 1. A two–layer structure with periodic interface, (6.1). (For interpretation of the colors in the figure(s), the reader is referred to the web version of this article.)

where $\alpha_p := \alpha + 2\pi\, p/d$,

$$\gamma_p^{(u)} = \sqrt{(k^{(u)})^2 - \alpha_p^2}, \quad \mathrm{Im}(\gamma_p^{(u)}) \geq 0,$$

and the "propagating modes" are

$$\mathcal{U}^{(u)} = \left\{ p \in \mathbf{Z} \mid \alpha_p^2 < \left(k^{(u)}\right)^2 \right\}.$$

If we choose an "artificial boundary" at $z = a > |g|_{L^\infty}$ and consider Dirichlet data there, $u_a(x) := u(x,a)$, then it is a simple matter to see that

$$u(x,z) = \sum_{p=-\infty}^{\infty} \hat{u}_{a,p} e^{i\alpha_p x} e^{i\gamma_p^{(u)}(z-a)}.$$

From this we can compute Neumann data, $\tilde{u}_a(x) := -(\partial_z u)(x,a)$,

$$\tilde{u}_a(x) = \sum_{p=-\infty}^{\infty} (-i\gamma_p^{(u)}) \hat{u}_{a,p} e^{i\alpha_p x},$$

and define the "Dirichlet–Neumann Operator" (DNO)

$$T^{(u)} : u_a \to \tilde{u}_a,$$

which is an order–one Fourier multiplier given by

$$T^{(u)}[u_a(x)] = \sum_{p=-\infty}^{\infty} (-i\gamma_p^{(u)}) \hat{u}_{a,p} e^{i\alpha_p x} = (-i\gamma_D^{(u)}) u_a(x).$$

With this we can enforce the outgoing wave condition transparently via the condition

$$\partial_z u + T^{(u)} u = 0, \quad z = a.$$

In a similar way we can enforce an outgoing (downward propagating) wave condition at an artificial boundary $z = -b < -|g|_{L^\infty}$

$$\partial_z u - T^{(w)} u = 0, \quad z = -b,$$

where $T^{(w)} = -(i\gamma_D^{(w)})$.

2.2. Far field observation

While we advocate an inversion strategy based upon "far field" data measured quite near the unknown grating interface (giving rise to "near field measurement" [29,6]) it is unreasonable to expect on–surface measurements. To specify the data which we deem relevant we again consider the artificial boundary $z = a$ and the far field pattern, $u_a(x)$. For future use, we denote the well–defined far field map

$$L : [u]_{z=g} \to u_a,$$

which has a severely ill–conditioned inverse, reflecting the fundamental ill–posedness of this inverse problem.

3. Boundary formulation by a domain decomposition method

We now specify a non–overlapping Domain Decomposition Method (DDM) reformulation of our problem in terms of the (upper and lower) Dirichlet traces

$$U(x) := [u]_{z=g}, \quad W(x) := [w]_{z=g},$$

and their (exterior pointing, upper and lower) Neumann analogues

$$\tilde{U}(x) := [-\partial_N u]_{z=g} = [-\partial_z u + (\partial_x g)\partial_x u]_{z=g},$$
$$\tilde{W}(x) := [\partial_N w]_{z=g} = [\partial_z w - (\partial_x g)\partial_x w]_{z=g}.$$

The equations (2.1c) and (2.1d) now read

$$U - W = \zeta, \quad -\tilde{U} - \tau^2 \tilde{W} = \psi. \tag{3.1}$$

These two equations for four unknowns can be re–expressed in terms of two unknowns by using DNOs.

Definition 3.1. Given a sufficiently smooth deformation $g(x)$ (C^2 is enough [80]), the unique quasiperiodic solution of

$$\Delta u + \left(k^{(u)}\right)^2 u = 0, \qquad g(x) < z < a, \tag{3.2a}$$
$$u = U, \qquad z = g(x), \tag{3.2b}$$
$$\partial_z u - T^{(u)} u = 0, \qquad z = a, \tag{3.2c}$$

defines the DNO

$$G(g) : U \to \tilde{U}. \tag{3.3}$$

In a similar fashion we have.

Definition 3.2. Given a sufficiently smooth deformation $g(x)$ (C^2 is enough [80]), the unique quasiperiodic solution of

$$\Delta w + \left(k^{(w)}\right)^2 w = 0, \qquad -b < z < g(x), \tag{3.4a}$$
$$w = W, \qquad z = g(x), \tag{3.4b}$$
$$\partial_z w - T^{(w)} w = 0, \qquad z = -b, \tag{3.4c}$$

defines the DNO

$$J(g) : W \to \tilde{W}. \tag{3.5}$$

In terms of these (3.1) becomes

$$U - W = \zeta, \quad -G[U] - \tau^2 J[W] = \psi,$$

and, using the first equation to eliminate $W = U - \zeta$, we find

$$(G + \tau^2 J)[U] = -\psi + \tau^2 J[\zeta]. \tag{3.6}$$

4. The forward problem

We now pause to carefully define our "forward problem" so that our inversion strategy can be clearly stated. To begin, as we noted in the Introduction, the nature of the problem which we seek to simulate gives us a wealth of information. More specifically we know:

1. The structure is doubly layered so we need to identify only the *single* interface $z = g(x)$.
2. The composition of the two layers are known so we can consider $n^{(u)}$ and $n^{(w)}$ as knowns.
3. The period of the interface, d, and the mean observation distance, a, are known. This is not strictly true, but we assume that the error in these measurement is much less than that of other mistakes we make.

In any experiment we can vary the angle, θ, and wavelength, λ, of the incident radiation, $u^i(x,z)$. From this we define the wavenumbers

$$k_0 = 2\pi/\lambda, \quad k^{(u)} = n^{(u)}k_0, \quad k^{(w)} = n^{(w)}k_0, \tag{4.1}$$

which give

$$\alpha = k^{(u)}\sin(\theta), \quad \gamma^{(u)} = k^{(u)}\cos(\theta), \quad \gamma^{(w)} = k^{(w)}\cos(\theta). \tag{4.2}$$

For the forward problem we consider the interface $g(x)$ as input, and view the far–field pattern, $u_a(x)$, as the output, and denote by F the forward map

$$F : g \to u_a.$$

An evaluation of this function amounts to solving the two equations

$$(G + \tau^2 J)U = -\psi + \tau^2 J[\zeta], \tag{4.3a}$$

$$u_a = L[U], \tag{4.3b}$$

or

$$u_a = L\left[(G + \tau^2 J)^{-1}\left[-\psi + \tau^2 J[\zeta]\right]\right]. \tag{4.4}$$

As we mentioned in the Introduction, there are a wide array of numerical methods for evaluating this map from volumetric schemes such as Finite Difference [64], Finite Element [57], Discontinuous Galerkin [46], Spectral Element [33], and Spectral [43,95] methods, to surface methods like Boundary Integral Methods [32,93]. Clearly, once an algorithm for simulating the DNOs is prescribed, then F can be evaluated; we select an efficient and robust HOPS scheme, more specifically the FE method of Bruno & Reitich [18–20]. As we shall see, this implementation gives an efficient and well–conditioned algorithm for recovering the interface shape $z = g(x)$ in our framework.

4.1. The method of field expansions

We now specify the FE recursions to simulate solutions of (3.2) and (3.4), and compute the DNOs, (3.3) and (3.5). In brief, the approach begins with the assumption that the shape of the interface deformation $g(x)$ satisfies

$$g(x) = \varepsilon f(x), \quad \varepsilon \ll 1,$$

with f sufficiently smooth (for a rigorous proof in the case of C^2 profiles see [80,82], while Lipschitz interfaces are considered in [31,53]). We point out that the smallness assumption on ε can be removed by analytic continuation [81,54] which has been numerically implemented via Padé summation [19,79,82]. With this assumption the fields and DNOs can be shown to depend *analytically* upon the deformation size ε so that

$$u = u(x,z;\varepsilon f) = \sum_{n=0}^{\infty} u_n(x,z)\varepsilon^n, \quad w = w(x,z;\varepsilon f) = \sum_{n=0}^{\infty} w_n(x,z)\varepsilon^n, \tag{4.5}$$

and

$$G = G(\varepsilon f) = \sum_{n=0}^{\infty} G_n\varepsilon^n, \quad J = J(\varepsilon f) = \sum_{n=0}^{\infty} J_n\varepsilon^n. \tag{4.6}$$

The question now becomes: Can useful forms for the $\{u_n, w_n, G_n, J_n\}$ can be derived? We briefly describe the FE method for this purpose.

In the current context, we insert the expansions (4.5) into (3.2) and (3.4) and seek governing equations for the $\{u_n, w_n\}$. For instance, we find that the u_n must be α–quasiperiodic, upward–propagating solutions of the elliptic boundary value problem [18–20]

$$\Delta u_n + \left(k^{(u)}\right)^2 u_n = 0, \qquad z > 0, \tag{4.7a}$$

$$u_n = \delta_{n,0} U + Q_n, \qquad z = 0, \tag{4.7b}$$

$$\partial_z u_n + T^{(u)} u_n = 0, \qquad z = a, \tag{4.7c}$$

where

$$Q_n = -\sum_{\ell=0}^{n-1} F_{n-\ell} \partial_z^{n-\ell} u_\ell(x,0), \quad F_n := \frac{f^n}{n!},$$

and $\delta_{n,\ell}$ is the Kronecker delta function. In a similar fashion

$$\begin{aligned} G[U] &= [-\partial_z u + (\varepsilon \partial_x f)\partial_x u]_{z=\varepsilon f(x)} \\ &= \sum_{n=0}^{\infty} -\partial_z u_n(x, \varepsilon f)\varepsilon^n + \varepsilon(\partial_x f) \sum_{n=0}^{\infty} \partial_x u_n(x, \varepsilon f)\varepsilon^n \\ &= \sum_{n=0}^{\infty}\sum_{m=0}^{\infty} -\partial_z \partial_z^m u_n(x,0) F_m \varepsilon^m \varepsilon^n + \varepsilon(\partial_x f) \sum_{n=0}^{\infty}\sum_{m=0}^{\infty} \partial_x \partial_z^m u_n(x,0) F_m \varepsilon^m \varepsilon^n \\ &= \sum_{n=0}^{\infty} \left(\sum_{m=0}^{n} -\partial_z^{n+1-m} u_m(x,0) F_{n-m} + \varepsilon(\partial_x f) \sum_{m=0}^{n-1} \partial_x \partial_z^{n-1-m} u_m(x,0) F_{n-1-m} \right) \varepsilon^n, \end{aligned}$$

so that [79,82]

$$G_n[U] = -\partial_z u_n(x,0) - \sum_{m=0}^{n-1} \left\{ \partial_z^{n+1-m} u_m(x,0) F_{n-m} + (\partial_x f)\partial_x \partial_z^{n-1-m} u_m(x,0) F_{n-1-m} \right\}. \tag{4.8}$$

The classical Rayleigh expansions [90,97], cf. (2.2), provide solutions

$$u_n(x,z) = \sum_{p=-\infty}^{\infty} \hat{u}_{n,p} e^{i\alpha_p x + i\gamma_p^{(u)} z},$$

and the $\{\hat{u}_{n,p}\}$ are determined recursively from the boundary conditions, (4.7b), beginning, at order zero, with

$$\hat{u}_{0,p} = \hat{U}_p.$$

Once the these $\{\hat{u}_{n,p}\}$ are discovered it is a simple matter to compute the G_n from (4.8). While this effectively describes the FE approach, for more details we refer the reader to [18] (or, in the context of Laplace's equation, to the recent contributions [76,77]).

5. The inverse problem

We are now in a position to specify our inversion strategy. As we noted in § 4, we are safe in assuming that much is already known: A doubly layered structure separated by an unknown interface, $z = g(x)$, with known refractive indices, $\{n^{(u)}, n^{(w)}\}$, period, d, and mean observation distance, a. Thus, we set ourselves the problem of finding $g(x)$ given the observation triple

$$\{\theta, \lambda, u_a(x)\},$$

though, through the relations (4.1) and (4.2), these are equivalent to the alternative triple

$$\{\alpha, k^{(u)}, u_a(x)\}.$$

We adopt a nonlinear least squares philosophy [61,89] and seek to minimize the residual

$$R(g;x) := \begin{pmatrix} (G(g) + \tau^2 J(g))[U(g)] + \psi(g) - \tau^2 J(g)[\zeta(g)] \\ u_a(g) - L(g)[U(g)] \end{pmatrix}, \tag{5.1}$$

cf. (4.3).

Among several strategies we considered for this task, the most rewarding were the Gauss–Newton (GN) approach, and the Levenberg–Marquardt (LM) algorithm [61,89]. Each of these is an iterative strategy which, given an initial guess, g^0, updates the current iterate, g^k, by adding a correction, v^k, to give a better approximation

$$g^{k+1} = g^k + v^k.$$

In the case of GN, the correction solves the least–squares system

$$J^T J v^k = -J R(g^k), \quad J = R'(g^k),$$

[61,89]. By contrast, LM considers a "regularized" system

$$\left(J^T J + \lambda_k \text{diag}[J]\right) v^k = -J R(g^k), \quad J = R'(g^k),$$

and $\lambda_k \geq 0$ is chosen adaptively based upon the ratio of actual to predicted reduction in the objective function $R^T R$ [61,89]. More precisely, we considered the recently specified enhanced adaptive scheme presented in [98].

Remark 5.1. Of course a consideration of considerable weight is the computation of the Jacobian matrix R'. As it is a very expensive operation (in fact the GN and LM methods are designed precisely to avoid the computation of the Hessian matrix, R'', as mandated by Newton's Method) one must decide if the exact evaluation of the full Jacobian is necessary for the application at hand. In this contribution we used a simple first–order finite difference approximation of R' to great effect. It is goal of future research to investigate the benefits of a faithful evaluation of the *full* Jacobian in the spirit of [40,41].

6. Numerical results

We now demonstrate the efficiency and utility of our algorithm, using both GN and LM minimization algorithms, by comparing its performance to that of the method of Malcolm and Nicholls [67]. The profiles and parameters we selected match those of [67] in order to give a fair and accurate assessment of performance. In all cases reported, we used as input data $\{\alpha, k^{(u)}\}$ together with a well–resolved solution, $u_a(x)$, of the forward problem (4.4) at $N_x = 32$ equally spaced gridpoints using $N = 10$ Taylor orders of the approximation

$$G^N[U] := \sum_{n=0}^{N} G_n[U]\varepsilon^n \approx G[U].$$

6.1. Gauss–Newton results

We started with the analytic and $d = 2\pi$ periodic profile

$$g(x) = \varepsilon e^{\cos(2x)} \tag{6.1}$$

(see Fig. 1) as the interface shape between two dielectrics with physical parameters

$$\alpha = 0, \quad k^{(u)} = 1.1, \quad k^{(w)} = 5.5, \quad a = 1. \tag{6.2}$$

In Table 1 we display, as a function of the deformation size ε (column one), the number of iterations required to reach absolute error tolerance 10^{-7} (column two), and the absolute and relative L^∞ errors at this number of iterations (columns three and four, respectively). These are the same values of ε discussed in [67] which display numbers of iterations ranging from 4 to 13. These calculations were revisited for values of ε ten times as big which were beyond the capabilities of the algorithm presented in [67]. In Table 2 we display, as a function of interface size, the number of iterations required to reach absolute error tolerance 10^{-7}. Once again our new algorithm delivers excellent results with a moderate number of iterations.

The next two profiles, also considered by [67], were chosen based upon their utility in modeling ocean bathymetry [87]. The function

$$g(x) = \varepsilon \text{sech}(2x), \tag{6.3}$$

was chosen to model a Gaussian pulse (see Fig. 2), and

$$g(x) = \varepsilon \left\{\tanh(2(x + 3\pi/5)) - \tanh(2(x - 3\pi/5))\right\}, \tag{6.4}$$

was chosen to approximate a sandbar (see Fig. 3). For each of these profiles we chose the configuration

Table 1
Absolute and relative L^∞ errors of GN method for $g(x) = \varepsilon e^{\cos(2x)}$ with physical parameters (6.2) and absolute error tolerance $\tau = 10^{-7}$.

ε	Iterations	Absolute error	Relative error
0.001	2	5.12385×10^{-9}	1.88496×10^{-6}
0.002	2	1.70321×10^{-8}	3.13287×10^{-6}
0.003	2	2.29475×10^{-8}	2.81398×10^{-6}
0.004	2	1.82473×10^{-8}	1.6782×10^{-6}
0.005	2	1.48634×10^{-8}	1.09359×10^{-6}
0.006	2	6.86197×10^{-8}	4.2073×10^{-6}
0.007	2	4.92943×10^{-8}	2.59062×10^{-6}
0.008	2	8.3038×10^{-8}	3.81849×10^{-6}
0.009	2	5.53309×10^{-8}	2.26168×10^{-6}
0.010	2	4.17534×10^{-8}	1.53602×10^{-6}

Table 2
Absolute and relative L^∞ errors of GN method for $g(x) = \varepsilon e^{\cos(2x)}$ with physical parameters (6.2) and absolute error tolerance $\tau = 10^{-7}$.

ε	Iterations	Absolute error	Relative error
0.01	2	4.17534×10^{-8}	1.53602×10^{-6}
0.02	3	1.33778×10^{-8}	2.4607×10^{-7}
0.03	3	8.09949×10^{-9}	9.93212×10^{-8}
0.04	3	1.41296×10^{-8}	1.2995×10^{-7}
0.05	3	1.69508×10^{-8}	1.24717×10^{-7}
0.06	3	4.84962×10^{-9}	2.97346×10^{-8}
0.07	3	7.78258×10^{-9}	4.09007×10^{-8}
0.08	3	1.48791×10^{-8}	6.84214×10^{-8}
0.09	3	6.35049×10^{-9}	2.59579×10^{-8}
0.10	3	9.92956×10^{-9}	3.65288×10^{-8}

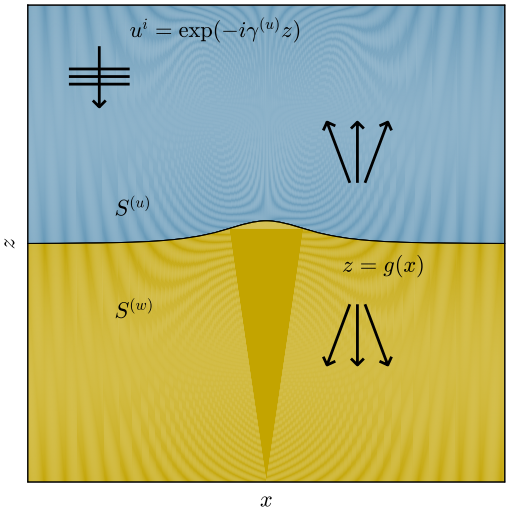

Fig. 2. A two–layer structure with Gaussian interface, (6.3).

$$\alpha = 0.2, \quad k^{(u)} = 1.3, \quad k^{(w)} = 6.8, \quad a = 1, \tag{6.5}$$

matching [67], and again took $N_x = 32$ equally–spaced grid points with a Taylor expansion of order $N = 10$. With our GN implementation we once again ran our algorithm and report our results in Tables 3, 4, 5, and 6. In Table 3 we considered the Gaussian pulse, (6.3), for values of ε studied in [67] and once again note the vastly superior performance of our new approach: 2 iterations versus 3–7. Again, for values of ε well beyond the capabilities of the method of [67], we show in Table 4 how our new method succeeds with ease. All of these are repeated for the sandbar profile, (6.4), for values in [67] (Table 5 showing 2 iterations versus 3–7 iterations in [67]) and beyond those in [67] (Table 6).

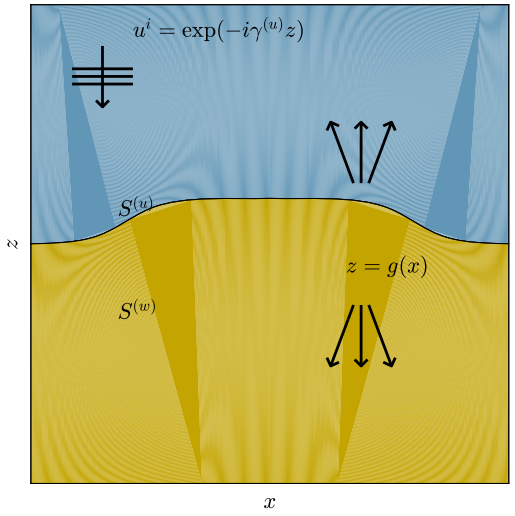

Fig. 3. A two–layer structure with sandbar interface, (6.4).

Table 3
Absolute and relative L^∞ errors of GN method for $g(x) = \varepsilon \text{sech}(2x)$ with physical parameters (6.5) and absolute error tolerance $\tau = 10^{-7}$.

ε	Iterations	Absolute error	Relative error
0.001	2	6.53059×10^{-9}	6.53059×10^{-6}
0.002	2	1.44806×10^{-8}	7.24031×10^{-6}
0.003	2	1.80531×10^{-8}	6.01771×10^{-6}
0.004	2	2.54028×10^{-8}	6.3507×10^{-6}
0.005	2	5.6527×10^{-9}	1.13054×10^{-6}
0.006	2	1.37405×10^{-8}	2.29009×10^{-6}
0.007	2	8.75834×10^{-9}	1.25119×10^{-6}
0.008	2	7.07984×10^{-9}	8.8498×10^{-7}
0.009	2	2.23095×10^{-8}	2.47883×10^{-6}
0.010	2	3.29825×10^{-8}	3.29825×10^{-6}

Table 4
Absolute and relative L^∞ errors of GN method for $g(x) = \varepsilon \text{sech}(2x)$ with physical parameters (6.5) and absolute error tolerance $\tau = 10^{-7}$.

ε	Iterations	Absolute error	Relative error
0.01	2	3.29825×10^{-8}	3.29825×10^{-6}
0.02	2	3.10684×10^{-8}	1.55342×10^{-6}
0.03	2	5.45511×10^{-8}	1.81837×10^{-6}
0.04	2	5.40971×10^{-8}	1.35243×10^{-6}
0.05	3	1.45434×10^{-8}	2.90869×10^{-7}
0.06	3	1.0168×10^{-8}	1.69467×10^{-7}
0.07	3	9.11842×10^{-8}	1.30263×10^{-6}
0.08	3	1.01959×10^{-8}	1.27449×10^{-7}
0.09	3	1.01747×10^{-8}	1.13053×10^{-7}
0.10	3	3.38578×10^{-9}	3.38578×10^{-8}

6.2. Levenberg–Marquardt results

We revisited all of the computations from the previous section in the context of the LM optimization strategy for the residual (5.1). The results of these experiments are given in Tables 7, 8, 9, 10, 11, 12. More specifically, in Table 7 we consider the analytic profile, (6.1), scaled by values of ε considered in [67] and note the superior performance which we enjoy. As before, we then took scalings ten times as large, with results shown in Table 8, which frustrated the algorithm in [67] that our new approach handled with relative ease.

For the Gaussian profile, (6.3), the results of our simulations are provided in Tables 9 and 10, and display the enhanced convergence rate and applicability of our new approach. To close, considering the sandbar profile, (6.4), we provide Tables 11 and 12 which tell much the same story of faster convergence and greater range of utility.

Table 5
Absolute and relative L^∞ errors of GN method for $g(x) = \varepsilon\{\tanh(2(x + 3\pi/5)) - \tanh(2(x - 3\pi/5))\}$ with physical parameters (6.5) and absolute error tolerance $\tau = 10^{-7}$.

ε	Iterations	Absolute error	Relative error
0.001	2	2.1134×10^{-8}	1.05783×10^{-5}
0.002	2	1.85757×10^{-8}	4.64886×10^{-6}
0.003	2	1.16117×10^{-8}	1.93734×10^{-6}
0.004	2	2.2996×10^{-8}	2.87755×10^{-6}
0.005	2	7.3449×10^{-8}	7.35271×10^{-6}
0.006	2	6.2667×10^{-8}	5.2278×10^{-6}
0.007	2	6.72537×10^{-8}	4.80894×10^{-6}
0.008	2	4.65598×10^{-8}	2.91309×10^{-6}
0.009	2	7.12626×10^{-8}	3.96324×10^{-6}
0.010	2	4.89571×10^{-8}	2.45046×10^{-6}

Table 6
Absolute and relative L^∞ errors of GN method for $g(x) = \varepsilon\{\tanh(2(x + 3\pi/5)) - \tanh(2(x - 3\pi/5))\}$ with physical parameters (6.5) and absolute error tolerance $\tau = 10^{-7}$.

ε	Iterations	Absolute error	Relative error
0.01	2	4.89571×10^{-8}	2.45046×10^{-6}
0.02	3	1.3441×10^{-8}	4.64886×10^{-6}
0.03	3	9.33326×10^{-9}	1.5572×10^{-7}
0.04	3	8.14999×10^{-9}	1.01983×10^{-7}
0.05	3	5.14035×10^{-9}	5.14582×10^{-8}
0.06	3	5.96408×10^{-9}	4.97535×10^{-8}
0.07	3	3.86656×10^{-9}	2.76477×10^{-8}
0.08	3	6.73874×10^{-9}	4.21619×10^{-8}
0.09	3	4.2248×10^{-9}	2.34961×10^{-8}
0.10	3	7.67753×10^{-9}	3.84285×10^{-8}

Table 7
Absolute and relative L^∞ errors of LM method for $g(x) = \varepsilon e^{\cos(2x)}$ with physical parameters (6.2) and absolute error tolerance $\tau = 10^{-7}$.

ε	Iterations	Absolute error	Relative error
0.001	2	7.04262×10^{-9}	2.59084×10^{-6}
0.002	2	1.2649×10^{-8}	2.32666×10^{-6}
0.003	2	4.30004×10^{-8}	5.27299×10^{-6}
0.004	3	5.56464×10^{-9}	5.11779×10^{-7}
0.005	3	3.04016×10^{-9}	2.23683×10^{-7}
0.006	3	3.30447×10^{-9}	2.02608×10^{-7}
0.007	3	6.61107×10^{-9}	3.4744×10^{-7}
0.008	3	2.83708×10^{-9}	1.30463×10^{-7}
0.009	3	3.65685×10^{-9}	1.49475×10^{-7}
0.010	3	4.73347×10^{-9}	1.74134×10^{-7}

Table 8
Absolute and relative L^∞ errors of LM method for $g(x) = \varepsilon e^{\cos(2x)}$ with physical parameters (6.2) and absolute error tolerance $\tau = 10^{-7}$.

ε	Iterations	Absolute error	Relative error
0.01	2	8.59926×10^{-8}	3.16349×10^{-6}
0.02	3	2.03003×10^{-9}	3.73404×10^{-8}
0.03	3	5.92628×10^{-9}	7.26719×10^{-8}
0.04	3	1.80464×10^{-8}	1.65973×10^{-7}
0.05	3	5.78422×10^{-8}	4.25579×10^{-7}
0.06	4	1.37597×10^{-8}	8.43649×10^{-8}
0.07	4	1.10804×10^{-8}	5.82324×10^{-8}
0.08	4	1.10195×10^{-8}	5.06729×10^{-8}
0.09	4	8.06238×10^{-9}	3.29554×10^{-8}
0.10	4	1.38966×10^{-8}	5.11227×10^{-8}

Table 9
Absolute and relative L^∞ errors of LM method for $g(x) = \varepsilon \text{sech}(2x)$ with physical parameters (6.5) and absolute error tolerance $\tau = 10^{-7}$.

ε	Iterations	Absolute error	Relative error
0.001	2	5.04942×10^{-9}	5.04942×10^{-6}
0.002	2	2.51027×10^{-8}	1.25513×10^{-5}
0.003	2	6.59102×10^{-8}	2.19701×10^{-5}
0.004	3	8.78783×10^{-9}	2.19696×10^{-6}
0.005	3	4.31915×10^{-9}	8.63831×10^{-7}
0.006	4	1.02421×10^{-8}	1.70702×10^{-6}
0.007	4	1.07042×10^{-8}	1.52916×10^{-6}
0.008	4	6.46297×10^{-9}	8.07871×10^{-7}
0.009	4	5.24258×10^{-9}	5.82509×10^{-7}
0.010	4	1.20323×10^{-8}	1.20323×10^{-6}

Table 10
Absolute and relative L^∞ errors of LM method for $g(x) = \varepsilon \text{sech}(2x)$ with physical parameters (6.5) and absolute error tolerance $\tau = 10^{-7}$.

ε	Iterations	Absolute error	Relative error
0.01	3	1.53242×10^{-8}	1.53242×10^{-6}
0.02	3	5.3662×10^{-9}	2.6831×10^{-7}
0.03	3	1.11801×10^{-8}	3.72669×10^{-7}
0.04	3	1.94143×10^{-8}	4.85359×10^{-7}
0.05	3	7.25992×10^{-8}	1.45198×10^{-6}
0.06	4	4.12845×10^{-9}	6.88075×10^{-8}
0.07	4	8.09638×10^{-9}	1.15663×10^{-7}
0.08	4	1.0433×10^{-8}	1.30413×10^{-7}
0.09	4	5.22884×10^{-9}	5.80982×10^{-8}
0.10	4	5.828×10^{-9}	5.828×10^{-8}

Table 11
Absolute and relative L^∞ errors of LM method for $g(x) = \varepsilon\{\tanh(2(x + 3\pi/5)) - \tanh(2(x - 3\pi/5))\}$ with physical parameters (6.5) and absolute error tolerance $\tau = 10^{-7}$.

ε	Iterations	Absolute error	Relative error
0.001	3	6.55021×10^{-9}	3.27859×10^{-6}
0.002	3	1.35846×10^{-8}	3.39976×10^{-6}
0.003	3	4.75449×10^{-9}	7.93258×10^{-7}
0.004	3	1.10139×10^{-8}	1.3782×10^{-6}
0.005	3	2.93964×10^{-9}	2.94276×10^{-7}
0.006	3	1.1869×10^{-8}	9.90133×10^{-7}
0.007	3	7.57871×10^{-9}	5.41912×10^{-7}
0.008	3	9.76948×10^{-9}	6.11242×10^{-7}
0.009	3	2.21945×10^{-8}	1.23434×10^{-6}
0.010	3	1.82724×10^{-8}	9.14593×10^{-7}

Table 12
Absolute and relative L^∞ errors of LM method for $g(x) = \varepsilon\{\tanh(2(x + 3\pi/5)) - \tanh(2(x - 3\pi/5))\}$ with physical parameters (6.5) and absolute error tolerance $\tau = 10^{-7}$.

ε	Iterations	Absolute error	Relative error
0.01	3	1.52832×10^{-8}	7.64973×10^{-7}
0.02	3	5.46978×10^{-9}	1.3689×10^{-7}
0.03	4	1.14338×10^{-8}	1.90766×10^{-7}
0.04	4	8.37588×10^{-9}	1.0481×10^{-7}
0.05	4	6.98388×10^{-9}	6.99131×10^{-8}
0.06	4	2.44196×10^{-8}	2.03713×10^{-7}
0.07	4	2.31178×10^{-8}	1.65303×10^{-7}
0.08	4	5.56971×10^{-8}	3.48477×10^{-7}
0.09	4	3.64979×10^{-8}	2.02982×10^{-7}
0.10	4	9.66565×10^{-8}	4.83797×10^{-7}

Acknowledgements

D.P.N. gratefully acknowledges support from the National Science Foundation through grant No. DMS-1522548.

References

[1] T. Arens, A. Kirsch, The factorization method in inverse scattering from periodic structures, Inverse Probl. 19 (5) (2003) 1195–1211.
[2] G.A. Baker Jr., P. Graves-Morris, Padé Approximants, 2nd edition, Cambridge University Press, Cambridge, 1996.
[3] G. Bao, A uniqueness theorem for an inverse problem in periodic diffractive optics, Inverse Probl. 10 (2) (1994) 335–340.
[4] G. Bao, A. Friedman, Inverse problems for scattering by periodic structures, Arch. Ration. Mech. Anal. 132 (1) (1995) 49–72.
[5] G. Bao, P. Li, J. Lv, Numerical solution of an inverse diffraction grating problem from phaseless data, J. Opt. Soc. Am. A 30 (2013) 293–299.
[6] G. Bao, P. Li, Y. Wang, Near-field imaging with far-field data, Appl. Math. Lett. 60 (2016) 36–42.
[7] G. Bao, P. Li, H. Wu, A computational inverse diffraction grating problem, J. Opt. Soc. Am. A 29 (2012) 394–399.
[8] A. Barnett, L. Greengard, A new integral representation for quasi-periodic scattering problems in two dimensions, BIT Numer. Math. 51 (2011) 67–90.
[9] J.-P. Bérenger, A perfectly matched layer for the absorption of electromagnetic waves, J. Comput. Phys. 114 (2) (1994) 185–200.
[10] J.-P. Bérenger, Evanescent waves in PML's: origin of the numerical reflection in wave-structure interaction problems, IEEE Trans. Antennas Propag. 47 (10) (1999) 1497–1503.
[11] T. Binford, D.P. Nicholls, N. Nigam, T. Warburton, Exact non–reflecting boundary conditions on general domains and hp-finite elements, J. Sci. Comput. 39 (2) (2009) 265–292.
[12] G. Bruckner, J. Cheng, M. Yamamoto, An inverse problem in diffractive optics: conditional stability, Inverse Probl. 18 (2) (2002) 415–433.
[13] G. Bruckner, J. Elschner, A two-step algorithm for the reconstruction of perfectly reflecting periodic profiles, Inverse Probl. 19 (2) (2003) 315–329.
[14] O. Bruno, B. Delourme, Rapidly convergent two–dimensional quasi–periodic Green function throughout the spectrum–including Wood anomalies, J. Comput. Phys. 262 (2014) 262–290.
[15] O.P. Bruno, A.G. Fernandez-Lado, Rapidly convergent quasi-periodic Green functions for scattering by arrays of cylinders–including Wood anomalies, Proc. R. Soc. A, Math. Phys. Eng. Sci. 473 (2199) (2017) 20160802.
[16] O.P. Bruno, M. Lyon, C. Pérez-Arancibia, C. Turc, Windowed Green function method for layered-media scattering, SIAM J. Appl. Math. 76 (5) (2016) 1871–1898.
[17] O.P. Bruno, C. Pérez-Arancibia, Windowed Green function method for the Helmholtz equation in the presence of multiply layered media, Proc. Math. Phys. Eng. Sci. 473 (2202) (2017) 20170161.
[18] O. Bruno, F. Reitich, Numerical solution of diffraction problems: a method of variation of boundaries, J. Opt. Soc. Am. A 10 (6) (1993) 1168–1175.
[19] O. Bruno, F. Reitich, Numerical solution of diffraction problems: a method of variation of boundaries. II. Finitely conducting gratings, Padé approximants, and singularities, J. Opt. Soc. Am. A 10 (11) (1993) 2307–2316.
[20] O. Bruno, F. Reitich, Numerical solution of diffraction problems: a method of variation of boundaries. III. Doubly periodic gratings, J. Opt. Soc. Am. A 10 (12) (1993) 2551–2562.
[21] O.P. Bruno, F. Reitich, Approximation of analytic functions: a method of enhanced convergence, Math. Comput. 63 (207) (1994) 195–213.
[22] O.P. Bruno, F. Reitich, Calculation of electromagnetic scattering via boundary variations and analytic continuation, Appl. Comput. Electromagn. Soc. J. 11 (1) (1996) 17–31.
[23] O.P. Bruno, F. Reitich, Boundary–variation solutions for bounded–obstacle scattering problems in three dimensions, J. Acoust. Soc. Am. 104 (5) (1998) 2579–2583.
[24] O.P. Bruno, F. Reitich, High-order boundary perturbation methods, in: Mathematical Modeling in Optical Science, in: Frontiers in Applied Mathematics Series, vol. 22, SIAM, Philadelphia, PA, 2001, pp. 71–109.
[25] O.P. Bruno, S.P. Shipman, C. Turc, S. Venakides, Superalgebraically convergent smoothly windowed lattice sums for doubly periodic Green functions in three-dimensional space, Proc. R. Soc. A, Math. Phys. Eng. Sci. 472 (2191) (2016) 20160255.
[26] F. Cakoni, D. Colton, A Qualitative Approach to Inverse Scattering Theory, Applied Mathematical Sciences, vol. 188, Springer, New York, 2014.
[27] F. Cakoni, D. Colton, H. Haddar, Inverse Scattering Theory and Transmission Eigenvalues, CBMS-NSF Regional Conference Series in Applied Mathematics, vol. 88, Society for Industrial and Applied Mathematics (SIAM), Philadelphia, PA, 2016.
[28] F. Cakoni, D. Colton, P. Monk, The Linear Sampling Method in Inverse Electromagnetic Scattering, CBMS-NSF Regional Conference Series in Applied Mathematics, vol. 80, Society for Industrial and Applied Mathematics (SIAM), Philadelphia, PA, 2011.
[29] T. Cheng, P. Li, Y. Wang, Near-field imaging of perfectly conducting grating surfaces, J. Opt. Soc. Am. A 30 (2013) 2473–2481.
[30] M.H. Cho, A. Barnett, Robust fast direct integral equation solver for quasi–periodic scattering problems with a large number of layers, Opt. Express 23 (2) (2015) 1775–1799.
[31] R. Coifman, Y. Meyer, Nonlinear harmonic analysis and analytic dependence, in: Pseudodifferential Operators and Applications, Notre Dame, Ind., 1984, Amer. Math. Soc., 1985, pp. 71–78.
[32] D. Colton, R. Kress, Inverse Acoustic and Electromagnetic Scattering Theory, 3rd edition, Applied Mathematical Sciences, vol. 93, Springer, New York, 2013.
[33] M.O. Deville, P.F. Fischer, E.H. Mund, High-Order Methods for Incompressible Fluid Flow, Cambridge Monographs on Applied and Computational Mathematics, vol. 9, Cambridge University Press, Cambridge, 2002.
[34] T.W. Ebbesen, H.J. Lezec, H.F. Ghaemi, T. Thio, P.A. Wolff, Extraordinary optical transmission through sub-wavelength hole arrays, Nature 391 (6668) (1998) 667–669.
[35] J. Elschner, G.C. Hsiao, A. Rathsfeld, Grating profile reconstruction based on finite elements and optimization techniques, SIAM J. Appl. Math. 64 (2) (2003/2004) 525–545.
[36] J. Elschner, G. Schmidt, Diffraction in periodic structures and optimal design of binary gratings. Part I: direct problems and gradient formulas, Math. Methods Appl. Sci. 21 (1998) 1297–1342.
[37] J. Elschner, G. Schmidt, Numerical solution of optimal design problems for binary gratings, J. Comput. Phys. 146 (2) (1998) 603–626.
[38] S. Enoch, N. Bonod, Plasmonics: From Basics to Advanced Topics, Springer Series in Optical Sciences, Springer, New York, 2012.
[39] Q. Fang, D.P. Nicholls, J. Shen, A stable, high–order method for three–dimensional bounded–obstacle scattering, J. Comput. Phys. 224 (2) (2007) 1145–1169.
[40] C. Fazioli, D.P. Nicholls, Parametric analyticity of functional variations of Dirichlet–Neumann operators, Differ. Integral Equ. 21 (5–6) (2008) 541–574.
[41] C. Fazioli, D.P. Nicholls, Stable computation of variations of Dirichlet–Neumann operators, J. Comput. Phys. 229 (3) (2010) 906–920.
[42] D. Givoli, Recent advances in the DtN FE method, Arch. Comput. Methods Eng. 6 (2) (1999) 71–116.

[43] D. Gottlieb, S.A. Orszag, Numerical Analysis of Spectral Methods: Theory and Applications, CBMS-NSF Regional Conference Series in Applied Mathematics, vol. 26, Society for Industrial and Applied Mathematics, Philadelphia, PA, 1977.
[44] L. Greengard, V. Rokhlin, A fast algorithm for particle simulations, J. Comput. Phys. 73 (2) (1987) 325–348.
[45] H.D. Han, X.N. Wu, Approximation of infinite boundary condition and its application to finite element methods, J. Comput. Math. 3 (2) (1985) 179–192.
[46] J.S. Hesthaven, T. Warburton, Nodal Discontinuous Galerkin Methods: Algorithms, Analysis, and Applications, Texts in Applied Mathematics, vol. 54, Springer, New York, 2008.
[47] F. Hettlich, Iterative regularization schemes in inverse scattering by periodic structures, Inverse Probl. 18 (3) (2002) 701–714.
[48] F. Hettlich, A. Kirsch, Schiffer's theorem in inverse scattering theory for periodic structures, Inverse Probl. 13 (2) (1997) 351–361.
[49] J. Homola, Surface plasmon resonance sensors for detection of chemical and biological species, Chem. Rev. 108 (2) (2008) 462–493.
[50] Y. Hong, D.P. Nicholls, A stable high-order perturbation of surfaces method for numerical simulation of diffraction problems in triply layered media, J. Comput. Phys. 330 (2017) 1043–1068.
[51] Y. Hong, D.P. Nicholls, A high–order perturbation of surfaces method for scattering of linear waves by periodic multiply layered gratings in two and three dimensions, J. Comput. Phys. 345 (2017) 162–188.
[52] Y. Hong, D.P. Nicholls, A high–order perturbation of surfaces method for vector electromagnetic scattering by doubly layered periodic crossed gratings, J. Comput. Phys. 372 (2018) 748–772.
[53] B. Hu, D.P. Nicholls, Analyticity of Dirichlet–Neumann operators on Hölder and Lipschitz domains, SIAM J. Math. Anal. 37 (1) (2005) 302–320.
[54] B. Hu, D.P. Nicholls, The domain of analyticity of Dirichlet–Neumann operators, Proc. R. Soc. Edinb. A 140 (2) (2010) 367–389.
[55] H. Im, S.H. Lee, N.J. Wittenberg, T.W. Johnson, N.C. Lindquist, P. Nagpal, D.J. Norris, S.-H. Oh, Template-stripped smooth Ag nanohole arrays with silica shells for surface plasmon resonance biosensing, ACS Nano 5 (2011) 6244–6253.
[56] X. Jiang, P. Li, Inverse electromagnetic diffraction by biperiodic dielectric gratings, Inverse Probl. 33 (2017) 085004.
[57] C. Johnson, Numerical Solution of Partial Differential Equations by the Finite Element Method, Cambridge University Press, Cambridge, 1987.
[58] C. Johnson, J.-C. Nédélec, On the coupling of boundary integral and finite element methods, Math. Comput. 35 (152) (1980) 1063–1079.
[59] J. Jose, L.R. Jordan, T.W. Johnson, S.H. Lee, N.J. Wittenberg, S.-H. Oh, Topographically flat substrates with embedded nanoplasmonic devices for biosensing, Adv. Funct. Mater. 23 (2013) 2812–2820.
[60] J.B. Keller, D. Givoli, Exact nonreflecting boundary conditions, J. Comput. Phys. 82 (1) (1989) 172–192.
[61] C.T. Kelley, Iterative Methods for Optimization, Frontiers in Applied Mathematics, vol. 18, Society for Industrial and Applied Mathematics (SIAM), Philadelphia, PA, 1999.
[62] A. Kirsch, Uniqueness theorems in inverse scattering theory for periodic structures, Inverse Probl. 10 (1) (1994) 145–152.
[63] R. Kress, Linear Integral Equations, 3rd edition, Springer-Verlag, New York, 2014.
[64] R.J. LeVeque, Finite Difference Methods for Ordinary and Partial Differential Equations: Steady-State and Time-Dependent Problems, Society for Industrial and Applied Mathematics (SIAM), Philadelphia, PA, 2007.
[65] N.C. Lindquist, T.W. Johnson, J. Jose, L.M. Otto, S.-H. Oh, Ultrasmooth metallic films with buried nanostructures for backside reflection-mode plasmonic biosensing, Ann. Phys. 524 (2012) 687–696.
[66] S.A. Maier, Plasmonics: Fundamentals and Applications, Springer, New York, 2007.
[67] A. Malcolm, D.P. Nicholls, A boundary perturbation method for recovering interface shapes in layered media, Inverse Probl. 27 (9) (2011) 095009.
[68] A. Malcolm, D.P. Nicholls, Operator expansions and constrained quadratic optimization for interface reconstruction: impenetrable acoustic media, Wave Motion 51 (2014) 23–40.
[69] D.M. Milder, An improved formalism for rough-surface scattering of acoustic and electromagnetic waves, in: Proceedings of SPIE – the International Society for Optical Engineering, San Diego, 1991, vol. 1558, Int. Soc. for Optical Engineering, Bellingham, WA, 1991, pp. 213–221.
[70] D.M. Milder, An improved formalism for wave scattering from rough surfaces, J. Acoust. Soc. Am. 89 (2) (1991) 529–541.
[71] D.M. Milder, H.T. Sharp, Efficient computation of rough surface scattering, in: Mathematical and Numerical Aspects of Wave Propagation Phenomena, Strasbourg, 1991, SIAM, Philadelphia, PA, 1991, pp. 314–322.
[72] D.M. Milder, H.T. Sharp, An improved formalism for rough surface scattering. II: numerical trials in three dimensions, J. Acoust. Soc. Am. 91 (5) (1992) 2620–2626.
[73] M. Moskovits, Surface–enhanced spectroscopy, Rev. Mod. Phys. 57 (3) (1985) 783–826.
[74] P. Nagpal, N.C. Lindquist, S.-H. Oh, D.J. Norris, Ultrasmooth patterned metals for plasmonics and metamaterials, Science 325 (2009) 594–597.
[75] D.P. Nicholls, A method of field expansions for vector electromagnetic scattering by layered periodic crossed gratings, J. Opt. Soc. Am. A 32 (5) (2015) 701–709.
[76] D.P. Nicholls, High–order perturbation of surfaces short course: boundary value problems, in: Lectures on the Theory of Water Waves, in: London Math. Soc. Lecture Note Ser., vol. 426, Cambridge Univ. Press, Cambridge, 2016, pp. 1–18.
[77] D.P. Nicholls, High–order perturbation of surfaces short course: analyticity theory, in: Lectures on the Theory of Water Waves, in: London Math. Soc. Lecture Note Ser., vol. 426, Cambridge Univ. Press, Cambridge, 2016, pp. 32–50.
[78] D.P. Nicholls, N. Nigam, Exact non-reflecting boundary conditions on general domains, J. Comput. Phys. 194 (1) (2004) 278–303.
[79] D.P. Nicholls, F. Reitich, Stability of high-order perturbative methods for the computation of Dirichlet-Neumann operators, J. Comput. Phys. 170 (1) (2001) 276–298.
[80] D.P. Nicholls, F. Reitich, A new approach to analyticity of Dirichlet-Neumann operators, Proc. R. Soc. Edinb., Sect. A 131 (6) (2001) 1411–1433.
[81] D.P. Nicholls, F. Reitich, Analytic continuation of Dirichlet-Neumann operators, Numer. Math. 94 (1) (2003) 107–146.
[82] D.P. Nicholls, F. Reitich, Shape deformations in rough surface scattering: improved algorithms, J. Opt. Soc. Am. A 21 (4) (2004) 606–621.
[83] D.P. Nicholls, F. Reitich, Shape deformations in rough surface scattering: cancellations, conditioning, and convergence, J. Opt. Soc. Am. A 21 (4) (2004) 590–605.
[84] D.P. Nicholls, J. Shen, A stable, high–order method for two–dimensional bounded–obstacle scattering, SIAM J. Sci. Comput. 28 (4) (2006) 1398–1419.
[85] D.P. Nicholls, J. Shen, A rigorous numerical analysis of the transformed field expansion method, SIAM J. Numer. Anal. 47 (4) (2009) 2708–2734.
[86] D.P. Nicholls, M. Taber, Joint analyticity and analytic continuation for Dirichlet–Neumann operators on doubly perturbed domains, J. Math. Fluid Mech. 10 (2) (2008) 238–271.
[87] D.P. Nicholls, M. Taber, Detection of ocean bathymetry from surface wave measurements, Eur. J. Mech. B, Fluids 28 (2) (2009) 224–233.
[88] D.P. Nicholls, V. Tammali, A high–order perturbation of surfaces (HOPS) approach to Fokas integral equations: vector electromagnetic scattering by periodic crossed gratings, Appl. Numer. Methods 101 (2016) 1–17.
[89] J. Nocedal, S.J. Wright, Numerical Optimization, 2nd edition, Springer Series in Operations Research and Financial Engineering, Springer, New York, 2006.
[90] R. Petit (Ed.), Electromagnetic Theory of Gratings, Springer-Verlag, Berlin, 1980.
[91] H. Raether, Surface Plasmons on Smooth and Rough Surfaces and on Gratings, Springer, Berlin, 1988.
[92] L. Rayleigh, On the dynamical theory of gratings, Proc. R. Soc. Lond. A 79 (1907) 399–416.
[93] F. Reitich, K. Tamma, State–of–the–art, trends, and directions in computational electromagnetics, Comput. Model. Eng. Sci. 5 (4) (2004) 287–294.

[94] S.O. Rice, Reflection of electromagnetic waves from slightly rough surfaces, Commun. Pure Appl. Math. 4 (1951) 351–378.
[95] J. Shen, T. Tang, L.-L. Wang, Spectral Methods: Algorithms, Analysis and Applications, Springer Series in Computational Mathematics, vol. 41, Springer, Heidelberg, 2011.
[96] H. Xu, E. Bjerneld, M. Käll, L. Börjesson, Spectroscopy of single hemoglobin molecules by surface enhanced Raman scattering, Phys. Rev. Lett. 83 (1999) 4357–4360.
[97] P. Yeh, Optical Waves in Layered Media, vol. 61, Wiley-Interscience, 2005.
[98] R. Zhao, J. Fan, On a new updating rule of the Levenberg–Marquardt parameter, J. Sci. Comput. 74 (2) (2018) 1146–1162.
[99] J. Zheng, J. Cheng, P. Li, S. Lu, Periodic surface identification with phase or phaseless near-field data, Inverse Probl. (2017) 115004.